NRIAG Journal of Astronomy and Geophysics 7 (2018) 279–296

Contents lists available at ScienceDirect

NRIAG Journal of Astronomy and Geophysics

journal homepage: www.elsevier.com/locate/nrjag

Full length article

Geoelectrical exploration of groundwater at West Dayrout Area, Assiut Governorate, Egypt

Th.H. Abdel Hafeez[a,*], H.S. Sabet[a], A.N. El-Sayed[b], M.A. Zayed[a]

[a] Geology Department, Science Faculty, Al-Azhar University, Cairo, Egypt
[b] Geophysics Department, Desert Research Center, Cairo, Egypt

ARTICLE INFO

Keywords:
Vertical electrical sounding (VES)
Water-bearing limestone
Geoelectrical exploration
Groundwater occurrences

ABSTRACT

The study area includes a western limestone plateau with a narrow strip of Nile Valley and extended between Latitudes 27° 27′–27° 43′ N and Longitudes 30° 25–30° 53′ E. The importance of this area increased after the construction of the Dayrout-Farafrah new road. This area was selected from the 1.5 million acre reclamation project. Reclamation depends on groundwater occurrence. So, this research will focus on groundwater exploration. The geoelectrical resistivity method was used for delineating of groundwater occurrence for recommending new localities for drilling wells. Thirty-four Schlumberger Vertical Electrical Soundings (VES) have been carried out with a maximum half current electrode spacing of 700 m. Results of the interpretation through the light of the Eocene aquifer characteristics along the study area indicates that the depth to water in Eocene aquifer varying from 66 to 120 m. and the best area for drilling wells is located in the southwestern, central and southern parts of the study area, where minimum depth to water and maximum groundwater resistivity values within Eocene aquifer are well-represented.

1. Introduction

The new reclamation projects are the main strategic targets of the Egyptian Government due to urbanization and high population density in Nile valley area. The investigation and evaluation of the groundwater are very important and essential for these reclamation projects (Salem, 2015). The new reclamation projects in the arid areas need a lot of efforts to explore and exploit new sources of groundwater (Mahmoud and Kotb, 2017). The study area (Fig. 1) is one of the promising areas for reclamation, especially after the construction of the Dayrout-Farafrah new road, which crosses it from east to west. This research will focus on groundwater occurrences at the western limestone plateau area. The geoelectrical resistivity method was used for detection of groundwater occurrences, and propose new localities for drilling wells.

2. Geologic setting

2.1. Geomorphologic features

Geomorphologically, there are three units dominated in the study area, from west to east as follow (Abdel Moneim et al., 2016), (Figs. 2a and 2b): Firstly, the recent alluvial plain which represents the old agricultural areas irrigated with surface water of the Nile and main canals such as El-Sohagiya, El-Ibrahimiya Canal, and Bahr Yousef. Secondly, the old alluvial plain which extends from the recent alluvial plain to the limestone plateau cliff and it is irrigated by groundwater. Finally, the limestone plateau which located at the boundary of Nile Valley from the eastern and western parts and it is consists of fractured limestone with sands and gravels at the surface.

2.2. Geologic exposures

The surface mappable rock units are represented by sedimentary rocks of Tertiary and Quaternary age, as shown on the surface geologic map (Fig. 3) (Conoco, 1987). Firstly, the Tertiary rocks are represented by Minia and Samalut Formations (Abou Heleika and Niesner, 2008). Minia Formation, composed of well-bedded white to gray aloveolinid lagoonal to marine limestone. The complete section of Minia Formation is 140 m (Said, 1990). Samalut Formation, overlays Minia Formation and mainly made up of white and chalky limestone with some marl and claystone interbeds and the thickness of Samalut Formation about 160 m (Said, 1990). Finally, the Quaternary rocks are represented by Holocene Nile silt, sand dunes, funglomerates and gravels

Peer review under responsibility of National Research Institute of Astronomy and Geophysics.
* Corresponding author.
E-mail address: Tharwat_geophysics@azhar.edu.eg (T.H. Abdel Hafeez).

https://doi.org/10.1016/j.nrjag.2018.07.004
Received 17 January 2018; Received in revised form 23 June 2018; Accepted 20 July 2018
Available online 08 September 2018

2.3. Structural elements

Structurally, there are two trends of faults that are bounded the Nile valley, these faults mainly take a direction of Gulf of Suez or Gulf of Aqaba (Youssef, 1968), and a number of fractures appear in (Fig. 3) also take these two directions. The area of NW-SE trending is playing a great role in recharging the Middle Eocene Limestone Aquifer (Shabana, 2010).

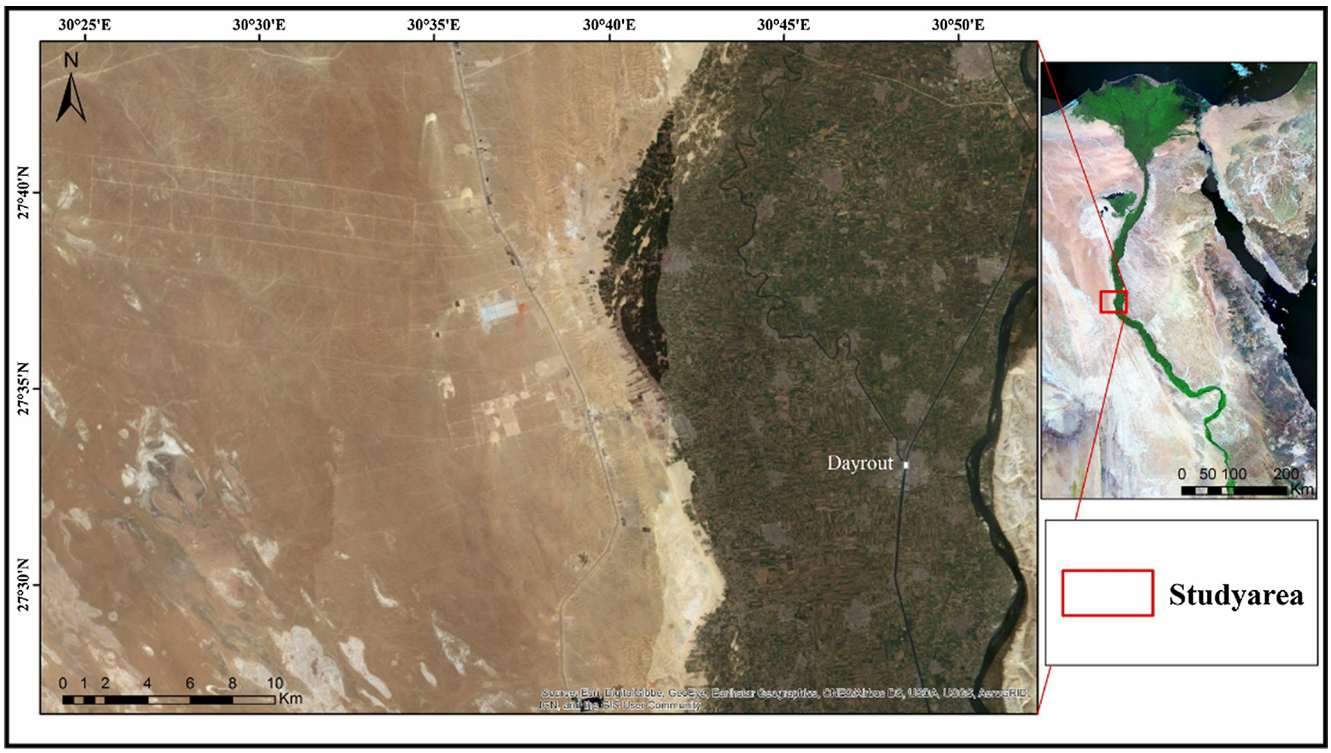

Fig. 1. Google earth map showing the location of the study area.

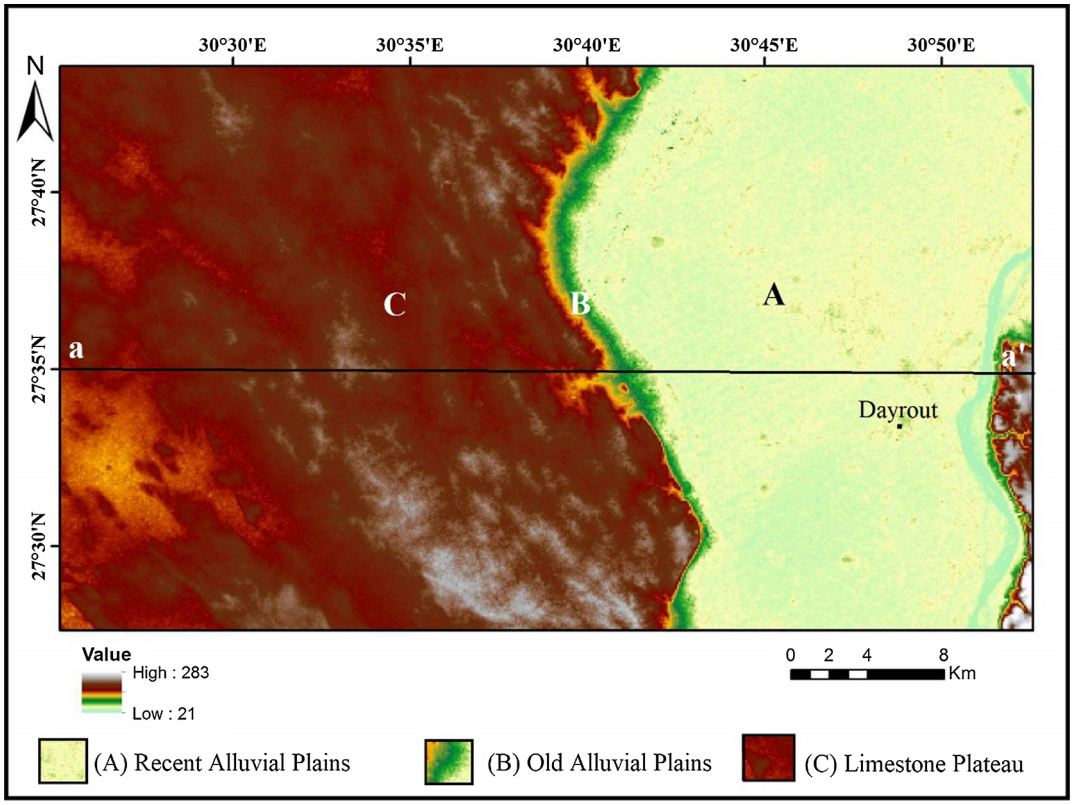

Fig. 2a. Geomorphology and digital elevation model of the study area.

Fig. 2b. Topographic profile a–a′ (digital elevation model).

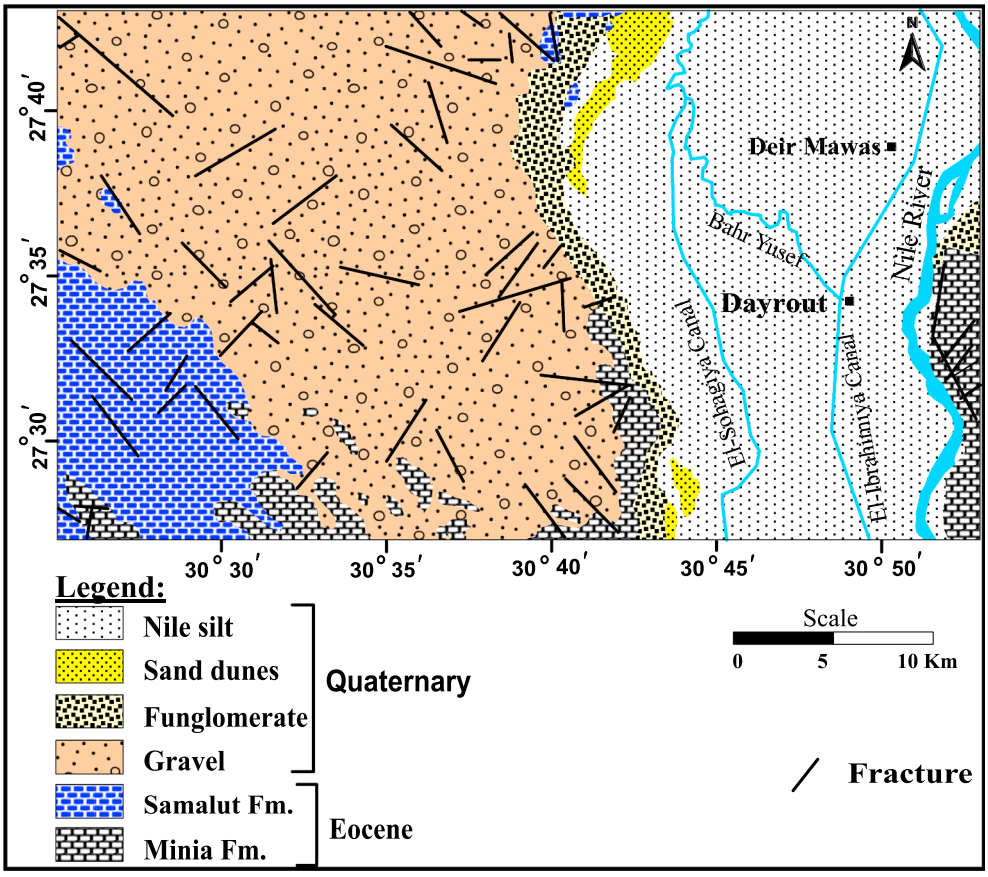

Fig. 3. Geological map of the study area. (After Conoco 1987).

3. Materials and methods

A geoelectrical survey was done using Schlumberger vertical electrical sounding (VES) technique during March 2016. This technique has been utilized for a wide variety of groundwater exploration studies (*e.g.* Mousa, 2003; Ibrahim, et al., 2004; Youssef et al.,2004; El-Deen et al., 2005; Alotaibi and Al-Amri, 2007; Abou Heleika and Niesner 2008; Mohamaden et al., 2009). Terameter SAS 1000 was used to carry out the survey applying the Schlumberger configuration (Fig. 4). The half electrode separation (AB/2) ranges between 1 and 700 m. As a foust of rule the maximum depth of penetration in such a configuration may reach third of the maximum current electrode separation (Abdel Fattah, 1990). This electrode separation is sufficient to reach the required depth of investigation, which fulfills the study object.

A total of thirty-four Vertical Electrical Soundings (VES) were measured, more or less in a grid pattern, along six E-W profiles perpendicular to three N-S profiles (Fig. 5). Some VES stations were measured beside water wells to be used during the quantitative interpretation.

The measured vertical electrical soundings are interpreted qualitatively and quantitatively to build a geoelectrical model. All the available data about the geologic and hydrogeologic settings were used to initiate this geoelectrical model. From the interpreted results which include the layers resistivities and thicknesses; nine geoelectric sections were constructed.

4. Results and discussion

The distribution of the measured vertical electrical soundings is illustrated in (Fig. 5) and interpreted as a qualitative and quantitative

Fig. 4. Data acquisition using Terrameter SAS 1000 resistivity meter instrument.

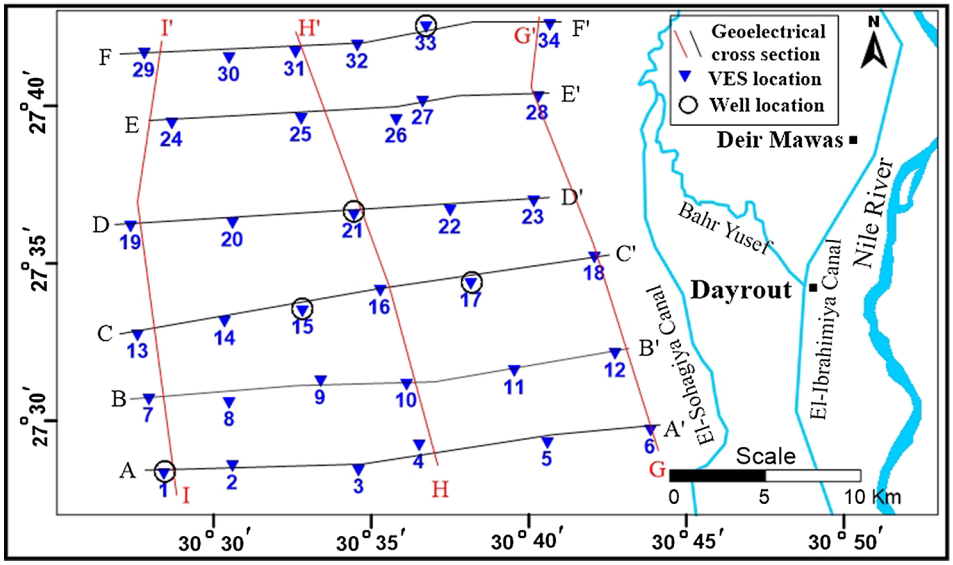

Fig. 5. VES's and cross-sections distribution in the study area.

interpretation. Generally, The results of the interpretation show that the number of interpreted units are nine geoelectrical layers and the true resistivity of these layers range between 1.5 and 8228 Ω m Also, the thicknesses of these layers vary from a sounding station to another (Table 1).

4.1. Qualitative interpretation

Examining the types of the collected apparent resistivity curves, a number of type curves and iso-apparent resistivity maps at different AB/2 separations constitute the main items for qualitative

Table 1
Resistivity and thickness results for each VES using IPI2 program

[a]	ρ1	h1	ρ2	h2	ρ3	h3	ρ4	h4	ρ5	h5	ρ6	h6	ρ7	h7
VES 1	6466	1	360	53.5	2.63	25.8	99	–	–	–	–	–	–	–
VES 2	6379	1.9	104	70	2.36	26	97.3	–	–	–	–	–	–	–
VES 3	5200	0.5	1846	1	198	4	50.7	19	549	61.8	104	–	–	–
VES 4	8319	0.5	2338	1.6	219	11.3	58.6	29.3	614	70.5	132	–	–	–
VES 5	8328	0.5	2333	2	281	11	50	29.3	532	59.3	118	–	–	–
VES 6	67.3	1.7	129	2	34.3	75	2.36	41	28	–	–	–	–	–
VES 7	3015	1.5	407	38.7	2.9	25.4	94.7	–	–	–	–	–	–	–
VES 8	11,941	0.6	542	43.5	3.3	28	78.3	–	–	–	–	–	–	–
VES 9	1611	0.5	293	4.6	60	33	513	60	106	–	–	–	–	–
VES 10	6500	0.45	233	4.6	55.7	28	479	62.8	113	–	–	–	–	–
VES 11	9732	0.5	2704	2	306	11	58.8	16.7	492	65.8	121	–	–	–
VES 12	28	3.3	176	3.4	31	64.8	2	35.3	30.6	–	–	–	–	–
VES 13	7615	0.7	2210	2.9	511	41	2.38	23.7	118	–	–	–	–	–
VES 14	4193	1.25	1705	1.6	171	6	51	16.5	426	54	94	–	–	–
VES 15	14.3	4	123	92	66	–	–	–	–	–	–	–	–	–
VES 16	6736	0.45	253	4.6	0.3	20.5	396	55	98	–	–	–	–	–
VES 17	6520	1.28	208	5.7	63	20	479	69	128	–	–	–	–	–
VES 18	28	3.4	228	3.4	28.6	58	2.2	35	24	–	–	–	–	–
VES 19	5517	1.25	1813	1.6	181	6	76	31	389	43	87	–	–	–
VES 20	6132	1.25	1920	1.6	198	6	64.5	36.4	404	45	101	–	–	–
VES 21	6500	0.45	350	4.3	51	22.6	314	75.5	106	–	–	–	–	–
VES 22	7720	0.9	109	3.9	51	12	407	63	107	–	–	–	–	–
VES 23	453	1	54	3.9	10.8	4.5	91	13.6	2	44	66	–	–	–
VES 24	5165	1.25	1720	2.2	196	11	80	24	4	10.7	309	41	66	
VES 25	3141	1	1505	1.7	177	8	50	33	355	41	92	–	–	–
VES 26	12,090	0.7	3390	2.9	249	8.6	40	32	486	53	97	–	–	–
VES 27	77	1	31.6	7.4	11	19.6	71.6	22.6	411	47	60	–	–	–
VES 28	105	1.3	15	7.8	1.6	11.8	20	14	2	39	45	–	–	–
VES 29	5165	1.25	1720	2.2	239	11	63	30	318	44	76	–	–	–
VES 31	2909	1	1330	1.7	136	8	27	4.5	86	42	407	40	96	
VES 32	2909	1	1330	1.8	155	6	43	37	460	45	82	–	–	–
VES 33	1677	0.9	292	6.7	78	21	20	32	436	41	51	–	–	–
VES 34	453	1.2	54	3.9	7.6	4.5	44	8	2.3	51	55	–	–	–

[a] (ρ) is a true resistivity & (h) is a thickness.

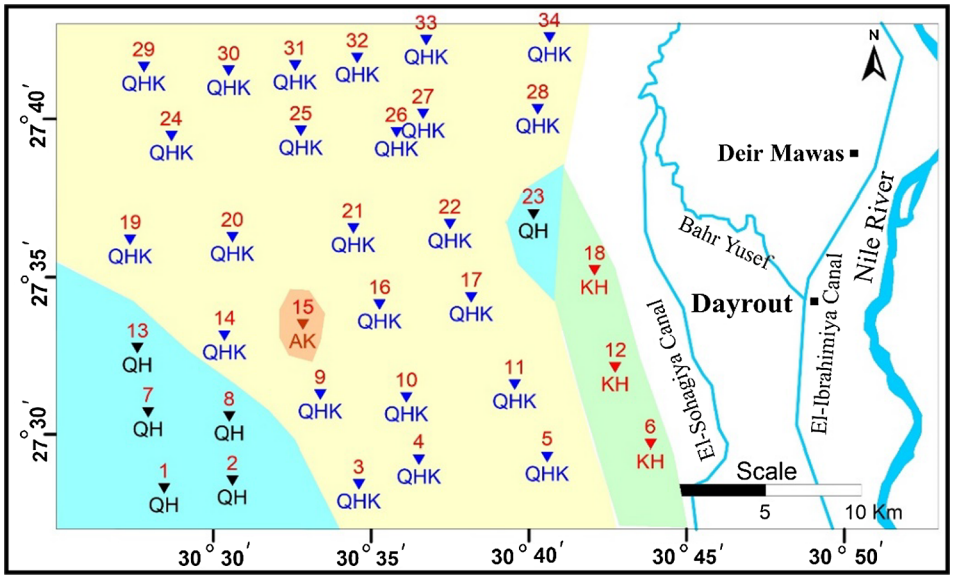

Fig. 6. Map showing the resistivity curve type distribution.

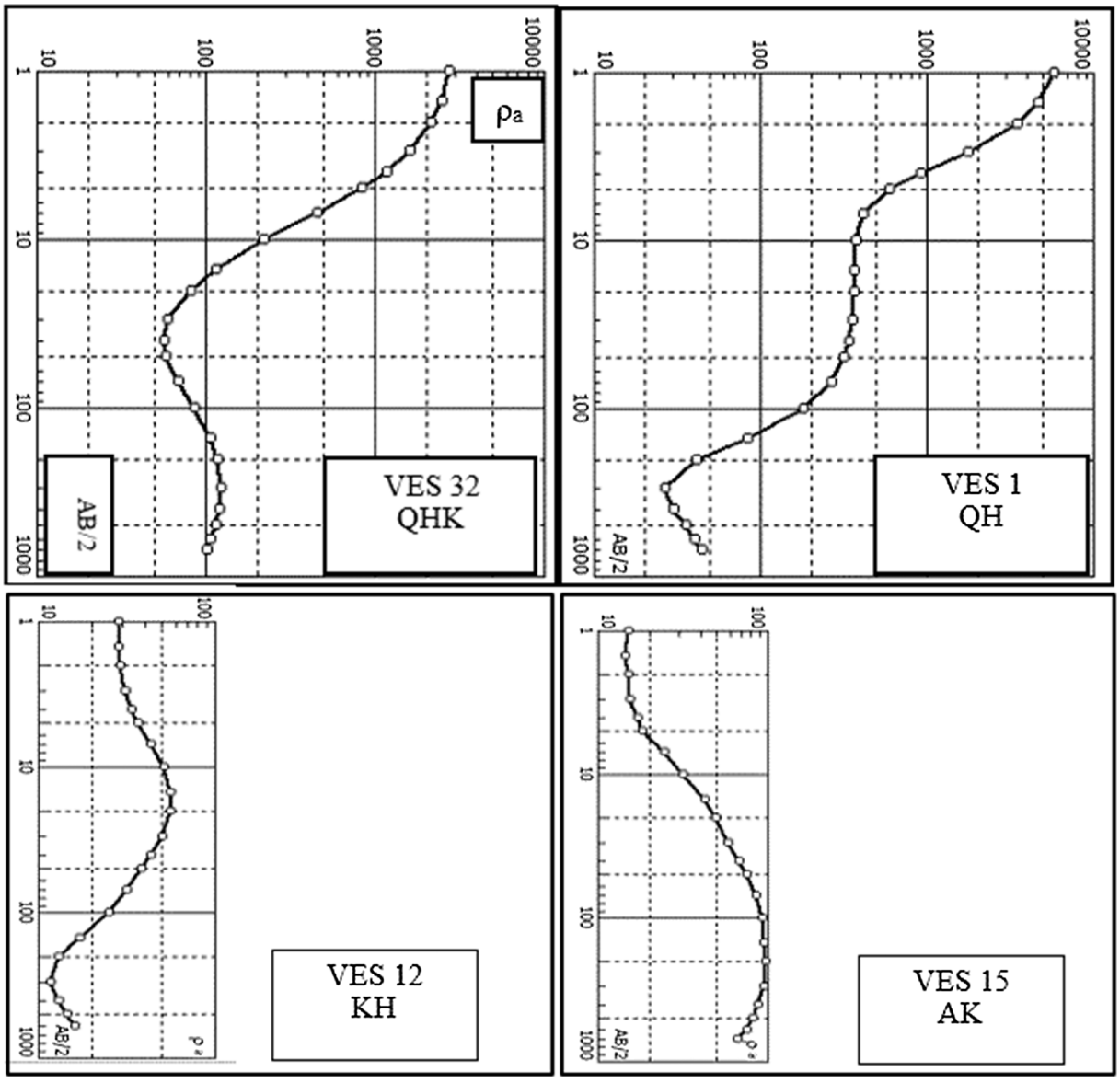

Fig. 7. Examples of different apparent resistivity type curve.

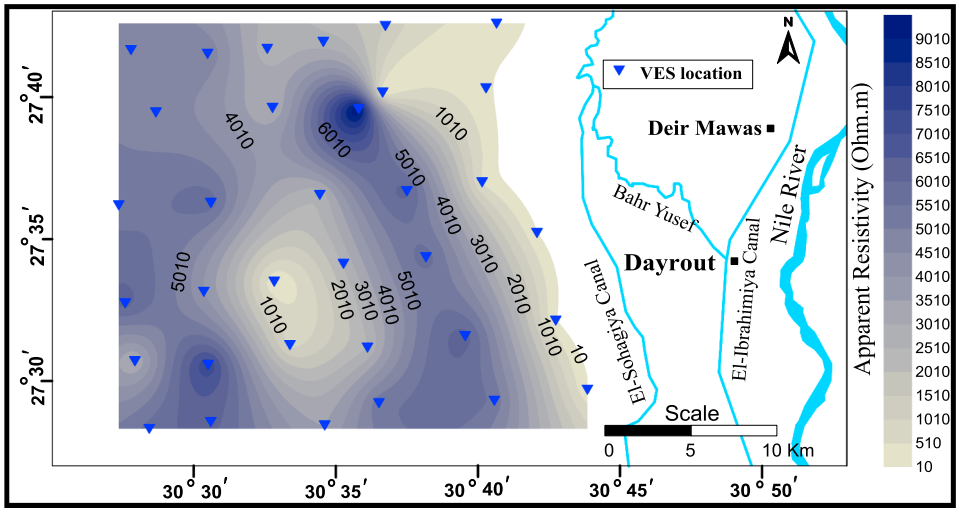

Fig. 8. Iso-apparent resistivity contour map at AB/2 = 1 m.

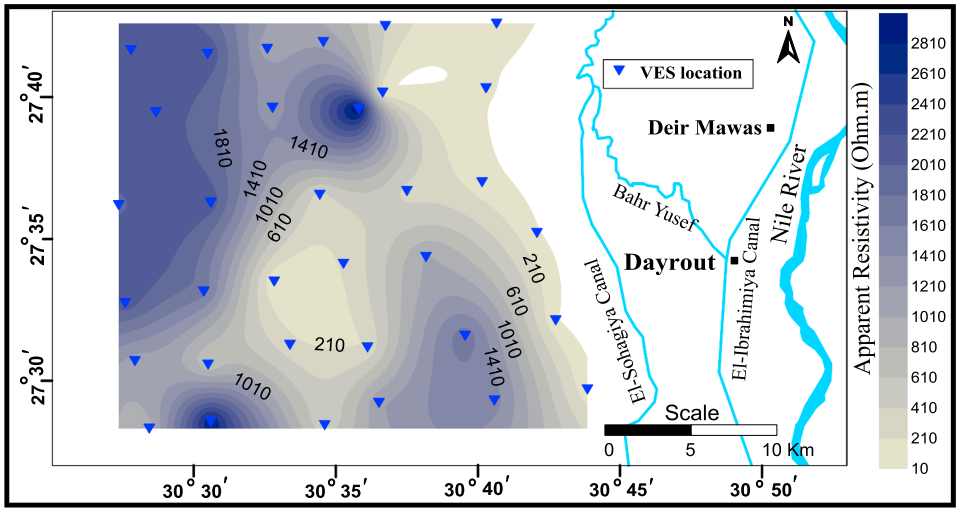

Fig. 9. Iso-apparent resistivity contour map at AB/2 = 4 m.

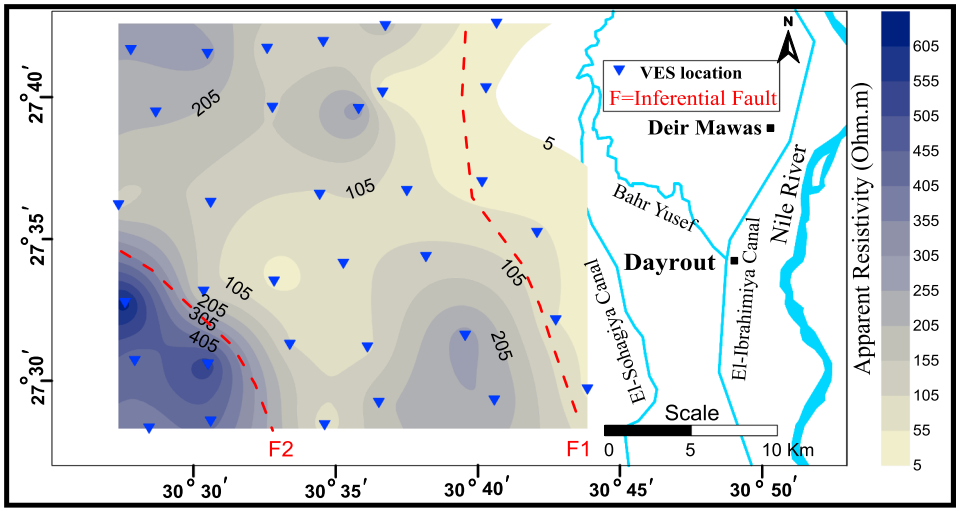

Fig. 10. Iso-apparent resistivity contour map at AB/2 = 15 m.

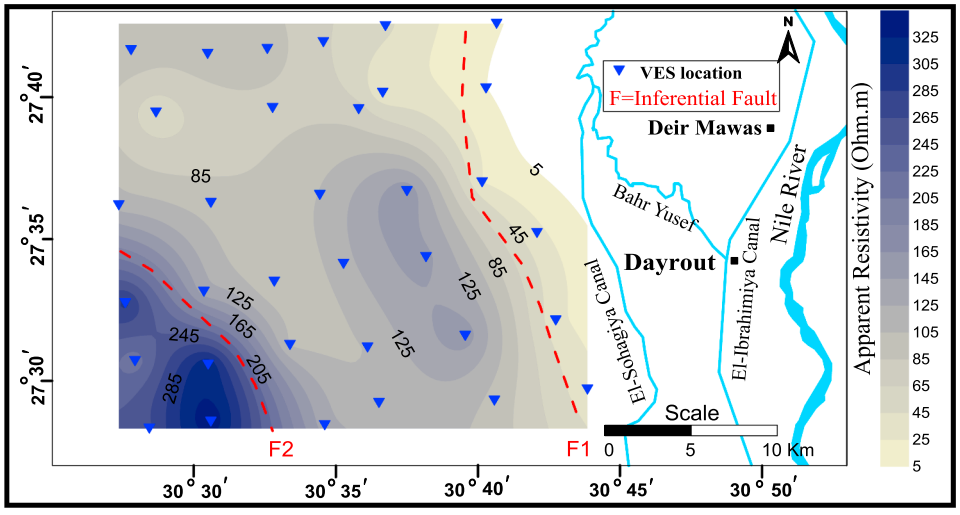

Fig. 11. Iso-apparent resistivity contour map at AB/2 = 70 m.

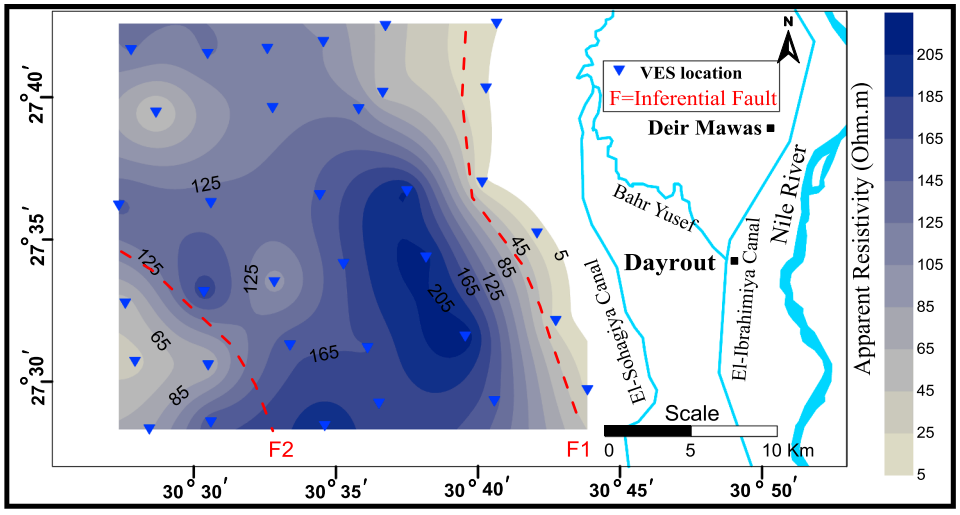

Fig. 12. Iso-apparent resistivity contour map at AB/2 = 150 m.

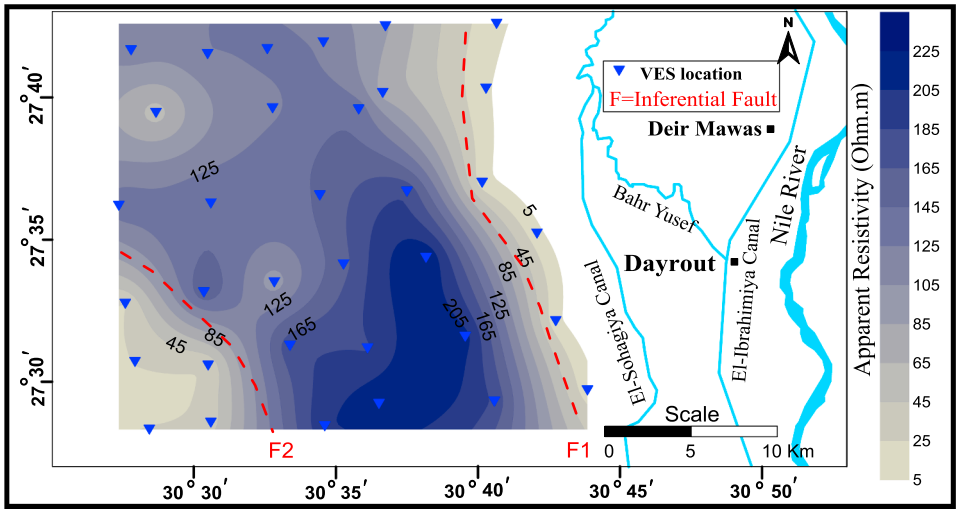

Fig. 13. Iso-apparent resistivity contour map at AB/2 = 300 m.

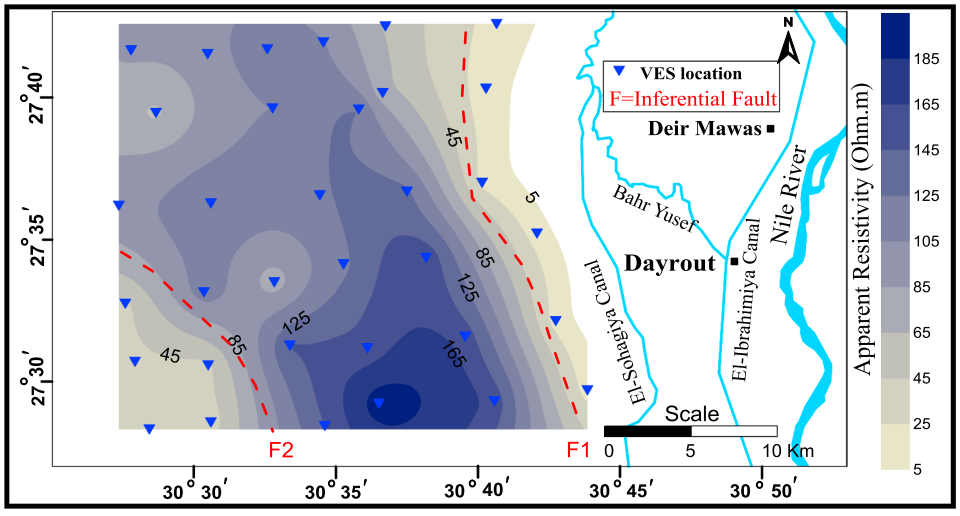

Fig. 14. Iso-apparent resistivity contour map at AB/2 = 600 m.

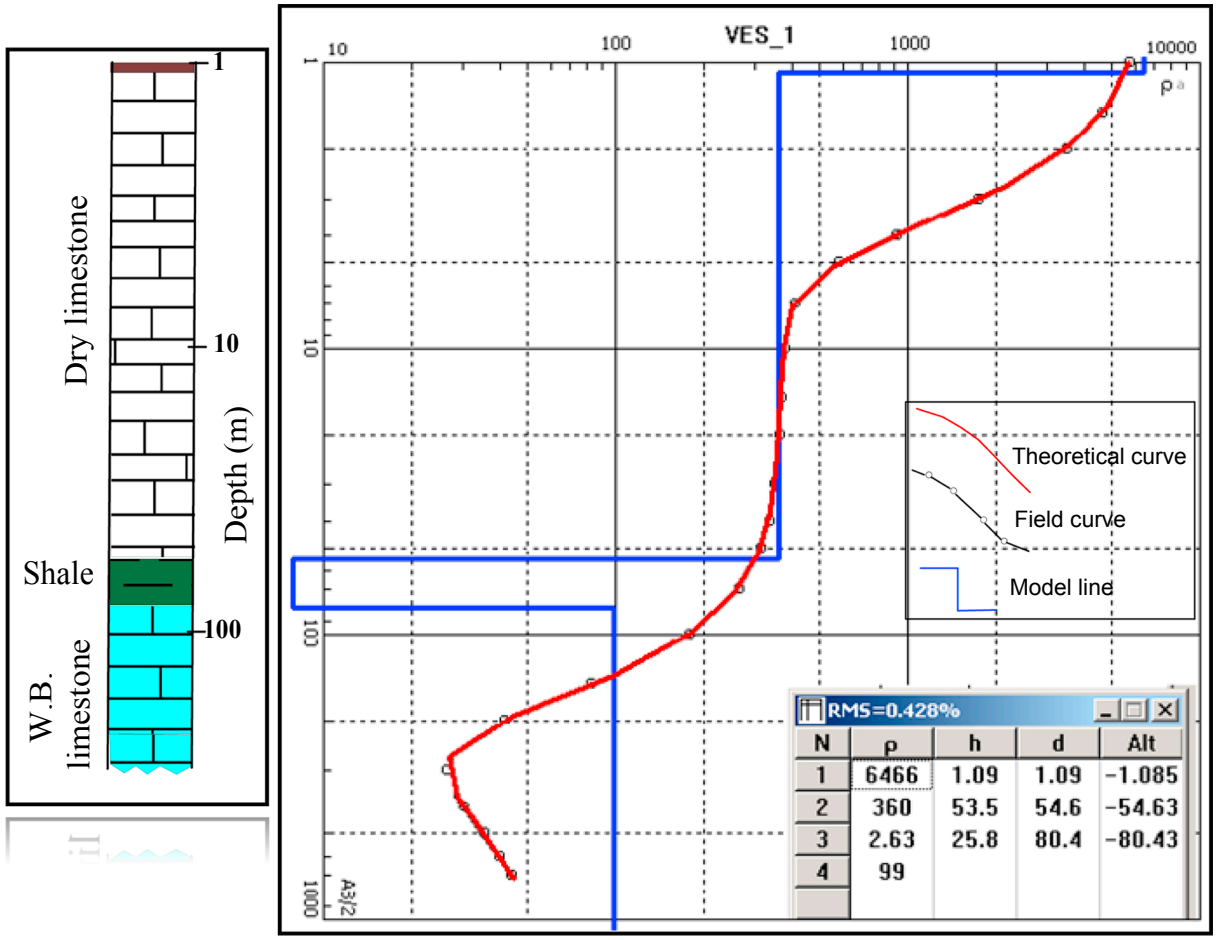

Fig. 15. The interpretation of VES No. 1 by using IPI2win Program.

interpretation.

4.1.1. Types of electrical resistivity sounding curve

The various types of the collected apparent resistivity curves give a preparatory impact on the resistivity distribution in the studied area. The presence of these different curve types give a direct indication of the resistivity due to the homogeneity of subsurface facies (Fig. 6).

Examining the collected apparent resistivity curves in the study area reveal that the observed curve types are related to geologic exposed rock units and the main common type of apparent resistivity curves in the area is the QHK (Fig. 7). The QHK type curve is represented by twenty-four sounding stations. These types of curves cover the most parts of the study area specially the area which covered by gravel and sand, comparing with geologic map (Fig. 3). This type curve described by the resistivity relation of ($\rho_1 > \rho_2 > \rho_3 < \rho_4 > \rho_5$).

The second one is QH type curve which is represented by six VES curves. They observed at southwestern area where Samalut Formation is exposed. This type curve is characterized by the resistivity relation of ($\rho_1 > \rho_2 > \rho_3 < \rho_4$).

The third curve type is KH which is represented by three VES curves, all of them are served at the Nile Valley area beside the limestone plateau. This resistivity type of curves described by the resistivity relation of ($\rho_1 < \rho_2 > \rho_3 < \rho_4$). Finally, there is only one curve represents AK curve type. This resistivity type of curves is described by the resistivity relation of ($\rho_1 < \rho_2 < \rho_3 > \rho_4$).

4.1.2. Iso-apparent resistivity contour maps

These maps were built to show that the lateral variations in the apparent electric resistivity at a different spacing (AB/2) which are related to different depths. There are number of maps are selected to show the apparent resistivity variation.

The apparent resistivity map at AB/2 of 1 m (Fig. 8) shows that the apparent resistivity has a wide range from 15 Ω m at VES 15 to 9735 Ω m at VES 26. This map indicates that the apparent resistivity has low values at the eastern part because the soundings are located in the Nile Valley, while the rest of soundings are located at western limestone plateau. The apparent resistivity map at AB/2 equals 4 m (Fig. 9) shows that the apparent resistivity values range from 17 Ω m at VES 15 to 3056 Ω m at VES 26. Apparent resistivity values at AB/2 equals 15 m (Fig. 10) shows that they range from 7.6 Ω m at VES station 28 to 632 Ω m at VES station 13. Whereas the apparent resistivity of AB/2 equals 70 m (Fig. 11) shows that they range from 5.3 Ω m at VES 28 to 341 Ω m at VES 2. The apparent resistivity map at AB/2 equals 150 m (Fig. 12) shows that the apparent resistivity values range from 6 Ω m at

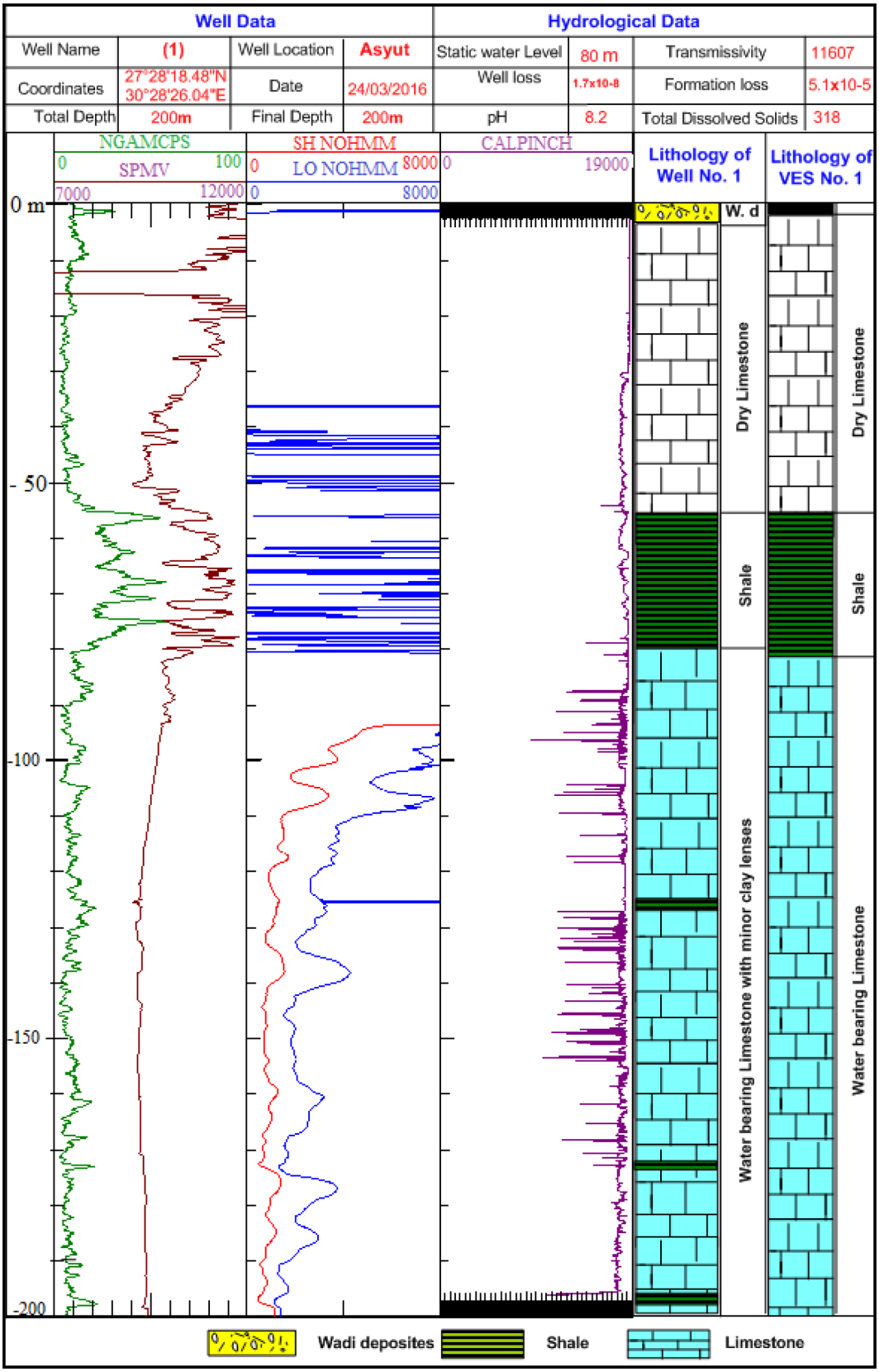

Fig. 16. Well-log data at VES No. 1 location.

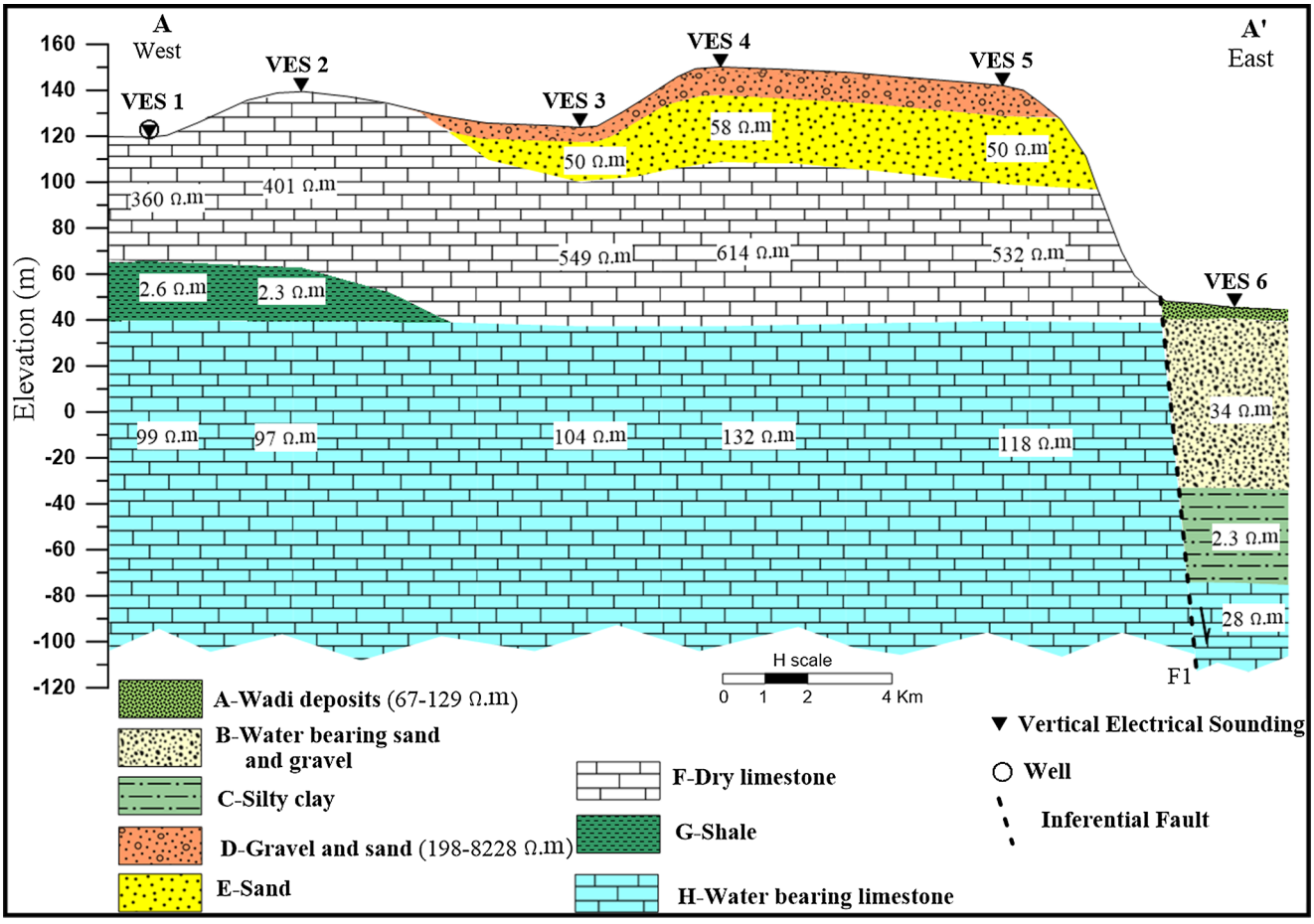

Fig. 17. Geoelectric resistivity cross-section A-A′.

VES 34 to 219 Ω m at VES 11. The apparent resistivity values at AB/2 equals 300 m (Fig. 13) shows that they range from 8.3 Ω m at VES station 28 to 225 Ω m at VES station 17. Whereas the apparent resistivity of AB/2 equals 600 m (Fig. 14) shows that they range from 14.5 Ω m at VES 28 to 196 Ω m at VES 4.

Generally, the apparent resistivity contour maps at different AB/2 spacing (1, 4, 15, 70, 150, 300 and 600 m) indicate that the apparent resistivity values at the same AB/2 spacing decreases towards the eastern direction that may be explained as a result of presence of an inferential fault (F1) between the Nile Valley and western limestone plateau. Also, there are abrupt changes in apparent resistivity at southwestern area may be due to the presence of an inferential fault (F2) between different rock types.

4.2. Quantitative interpretation

4.2.1. Geoelectrical cross-sections

Nine geoelectrical cross-sections have been constructed based on the results of the interpreted VES soundings (Figs. 17–25). The aim of these sections is to show the extension of the geoelectrical layers and the aquifers geometry in the investigated area. These sections reflect both lateral and vertical variations in lithology according to resistivity values. The best model for each sounding was constructed (Fig. 15) by using the geoelectrical information of boreholes and available well-log data (Fig. 16) which used for calibration.

The ranges of resistivity and thickness of each layer are listed in (Table 2). A description of these geoelectrical layers from top to bottom is given as the following:

- **Geoelectrical Layer (A):** This layer observed as a narrow strip at the western part of the Nile valley. It is represented by dry wadi deposits, which consists of sand and silt, and its resistivity values varying from 15 to 453 Ω m. The low resistivity value within this layer is due to that the increase of fine sediments such as fine silt lenses and the maximum thickness of this layer was 10 m at VES 28.
- **Geoelectrical Layer (B):** This layer underlays the layer (A) and it is consists of water-bearing sand and gravel, which represents a Quaternary aquifer extension in the area of study. Its resistivity values ranging from 20 to 90 Ω m and the maximum thickness of this layer was 73 m at VES 6.
- **Geoelectrical Layer (C):** This layer observed underlays the layer (B) at the western part of the Nile valley. It consists of siltyclay, which has a relatively low resistivity values varying from 2 to 2.3 Ω m. The thickness of this layer ranging from 34 m at VES 18 to 44 m at VES 23.
- **Geoelectrical Layer (D):** This layer has a wide distribution as a surface area at a central part of the study area from south to north. It is consists of sand and gravels, which has resistivity values varying from 76 to 8228 Ω m, this wide resistivity range is explained due to increasing of fine sediments such as fine sand downward and

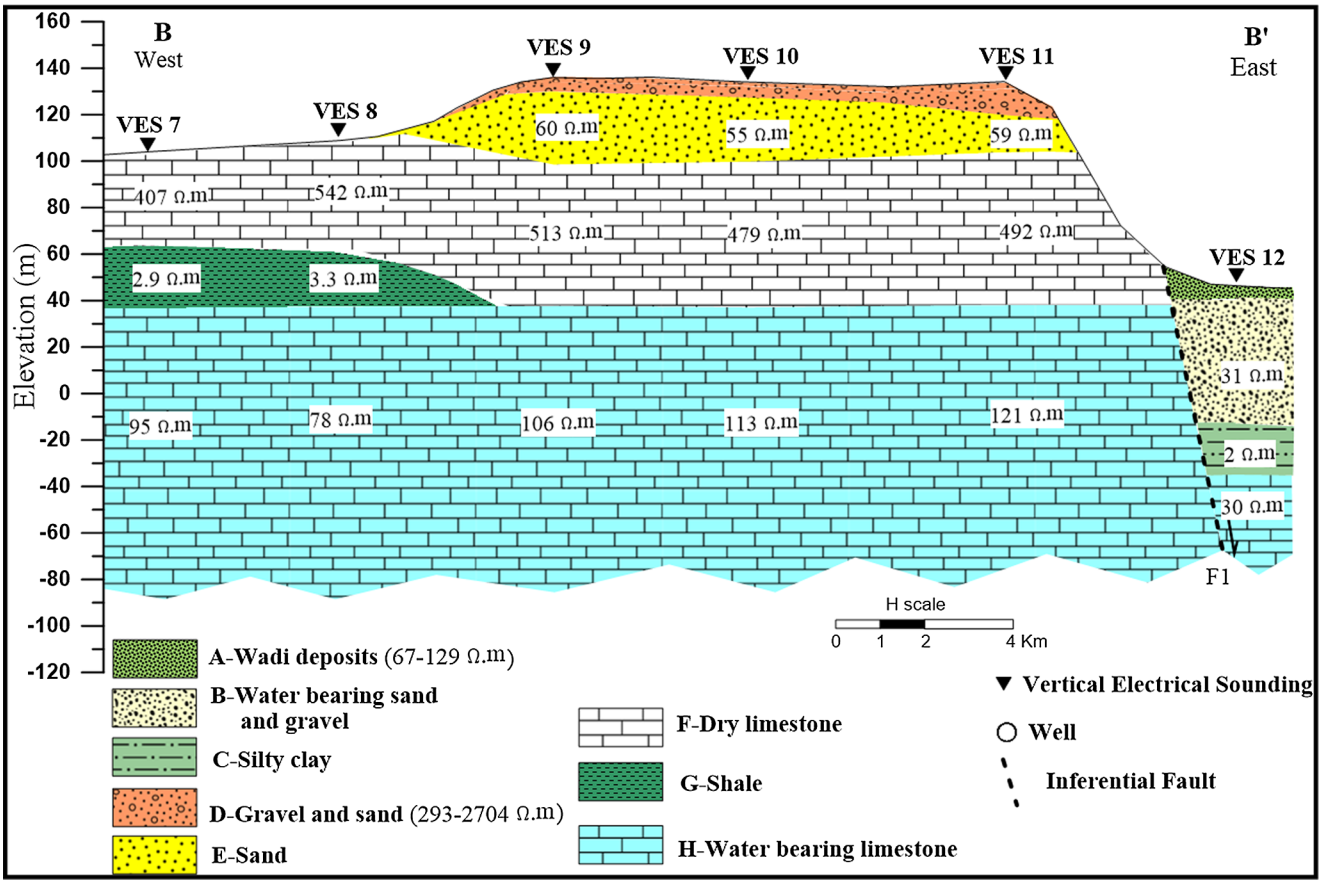

Fig. 18. Geoelectric resistivity cross-section B-B′.

presence of gravels contain limestone fragments in some localities. The thickness of this layer ranging from 5 m at VES 22 to 28 m at VES 33.

- **Geoelectrical Layer (E):** This layer underlay the gravel layer (D) and consists of sand. Its resistivity values varying from 20 to 123 Ω m. The thickness of this layer ranging from 12 m at VES 22 to 90 m at VES 15. The thickness increasing toward the extreme northern part and consist a polio-channel of sand (Fig. 19).
- **Geoelectrical Layer (F):** This layer underlain the sand layer (E) which has a wide distribution in the study area, and consists of dry Eocene limestone. It has resistivity values varying from 309 to 614 Ω m. The thickness of this layer ranging from 40 m at VES 7 to 70 m at VES 2.
- **Geoelectrical Layer (G):** This layer underlay the dry limestone layer (F) which observed in a southwest part of the study area and well log 1 (Fig. 16). It consists of dry Eocene shale, which has a relatively low resistivity values varying from 2.3 to 3.3 Ω m. The thickness of this layer ranging from 24 m at VES 13 to 27 m at VES 22.
- **Geoelectrical Layer (H):** This layer observed at whole regions of the study area and represents the main aquifer. It consists of water-bearing Eocene limestone. It has resistivity values varying from 24 to 132 Ω m Table 2: Resistivities, Thicknesses Ranges, and their Related Lithology.

4.2.2. Hydrogeologic setting

Based on the geoelectrical results, there are two water-bearing geoelectrical layers (B and H) which represent groundwater aquifers:

1. Quaternary Aquifer (Layer B).
2. Eocene Aquifer (Layer H).

A description of each aquifer is given as the following:

1. Quaternary Aquifer (Layer B)

This aquifer observed along the western part of the Nile valley. It is consists of water-bearing sand and gravel, which represents the Quaternary aquifer extension in the area of investigation. The resistivity values of this layer varying from 20 to 90 Ω m, and the maximum thickness was 73 m at VES 6 and decreases toward the northern part where the minimum thickness of 13 m at VES 23 is observed. It is completely faded at the extreme northern part (Fig. 23). This aquifer is underlain by siltyclay layer (C) which affected by two geoelectrical inferential faults (F4 and F5).

2. Eocene Aquifer (Layer H)

This aquifer observed all over the study area and represents the

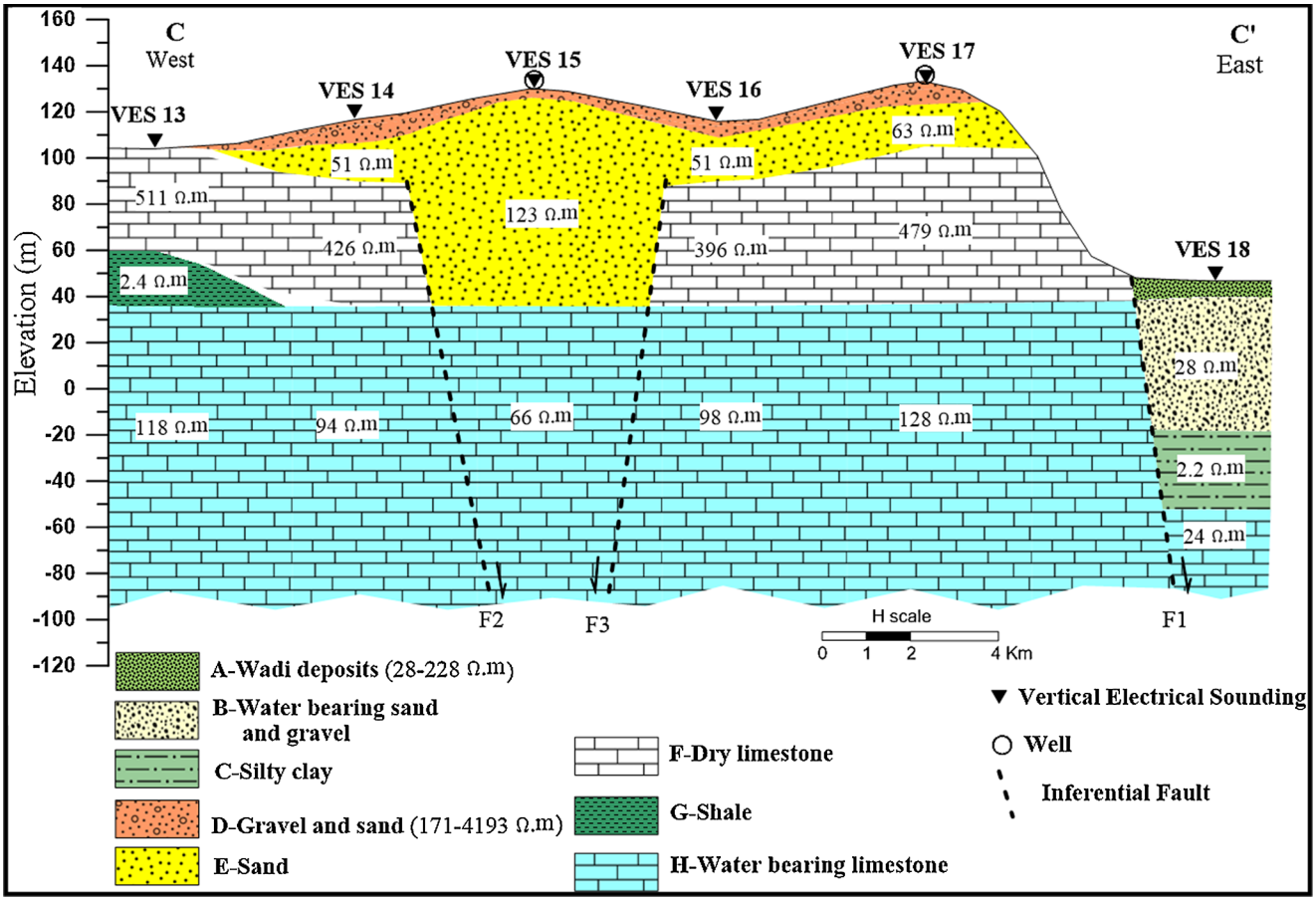

Fig. 19. Geoelectric resistivity cross-section C-C′.

main aquifer. It consists of water-bearing Eocene limestone. It has resistivity values varying from 24 to 132 Ω m The Iso-resistivity contour map (Fig. 26) of Eocene aquifer indicates that the maximum resistivity values observed at the southern and central parts, while the eastern regions have a relatively low resistivity values varying from 24 to 65 Ω m. The decreasing in resistivity values at the eastern parts is due to the presence of siltyclay layer (C) beside the Eocene aquifer as a structural effect between a western limestone plateau and Nile valley.

4.2.3. Depth to Eocene aquifer (Layer H) contour map

The depth of water-bearing layer which represents the Eocene aquifer of Minia Formation varies from 65 m to 120 m from the ground surface (Fig. 27). The minimum depth located at southwest and northeast parts (from 65 to 90 m), while the southeast regions have a maximum depth, which ranges from 90 to 120 m.

5. Conclusions

Based on the geoelectrical analysis, two water-bearing geoelectrical layers (B and H) which represent groundwater aquifers. The results of the current research give the following concluding remarks:

Firstly, Quaternary aquifer (Layer B) is observed as a narrow strip at the western part of the Nile valley. It consists of water-bearing sand and gravel, which represents the Quaternary aquifer extension in the area of investigation. It has resistivity values varying from 20 to 90 Ω m and the maximum thickness of this layer ranges between 73 m at VES 6 and decreases toward the northern part. It is completely faded at the extreme northern part. This aquifer is underlain by siltyclay layer (C) which is affected by two geoelectrical inferential faults (F4 and F5).

Secondly, Eocene aquifer (Layer H) dominating in the whole parts of

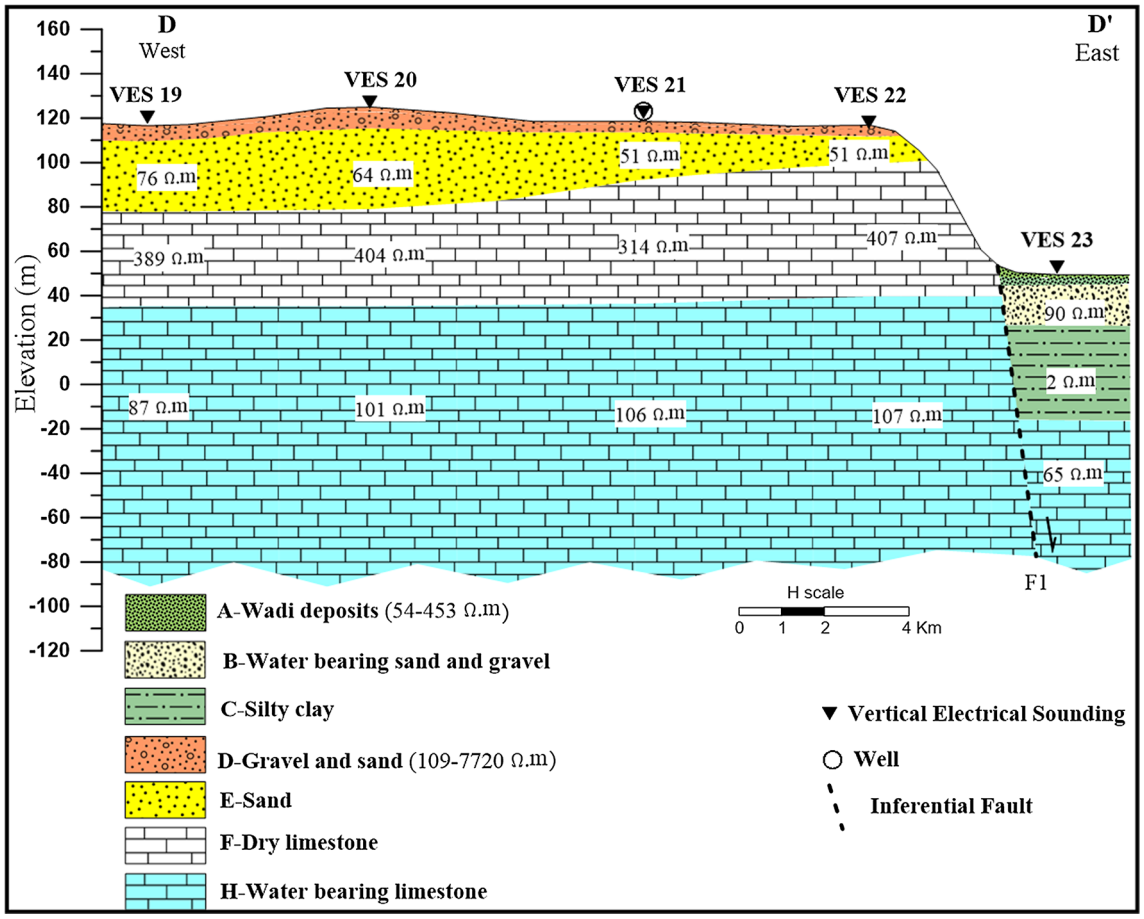

Fig. 20. Geoelectric resistivity cross-section D-D′.

the study area and represents the main aquifer. It consists of water-bearing Eocene limestone and has resistivity values varying from 24 to 132 Ω m The Iso-resistivity contour map of Eocene aquifer indicates that the maximum resistivity values observed in the southern and central parts, while the eastern regions have a relatively low resistivity values due to Nile valley stations.

Finally, Quaternary aquifer (Layer B) represents a narrow strip at the western part of the Nile valley, while Eocene aquifer has a wide distribution in the study area. The best areas for drilling wells in the Eocene aquifer are southwest, central and south regions where minimum depth to water and maximum groundwater resistivity values within Eocene aquifer are well represented, opposite to that at east and northeast areas.

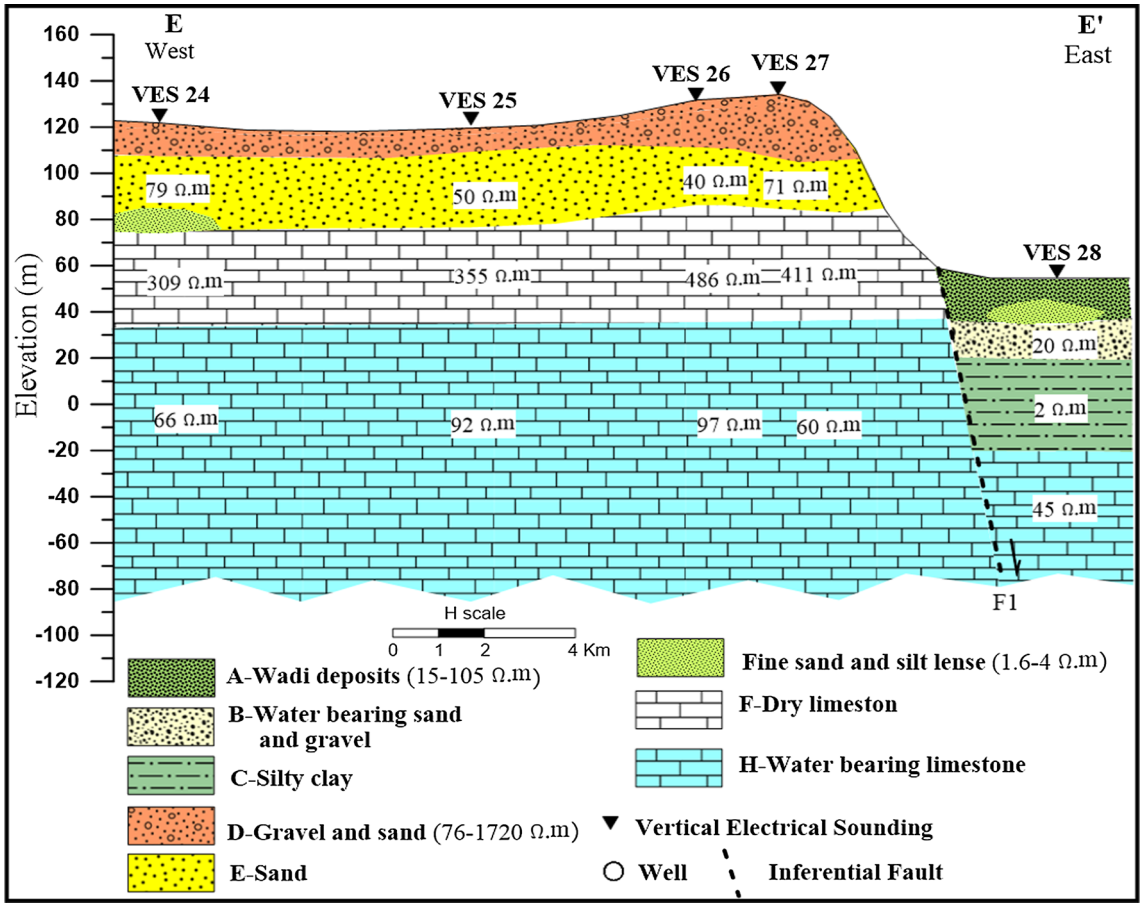

Fig. 21. Geoelectric resistivity cross-section E-E′.

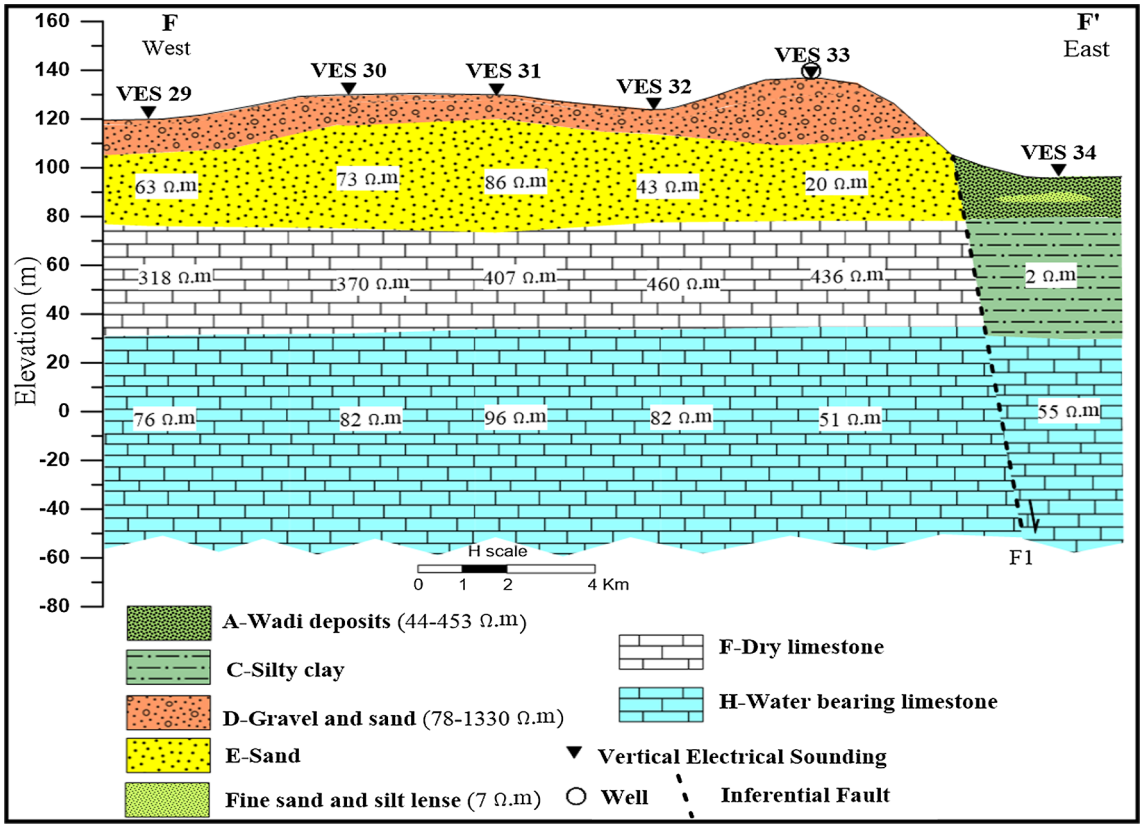

Fig. 22. Geoelectric resistivity cross-section F-F′.

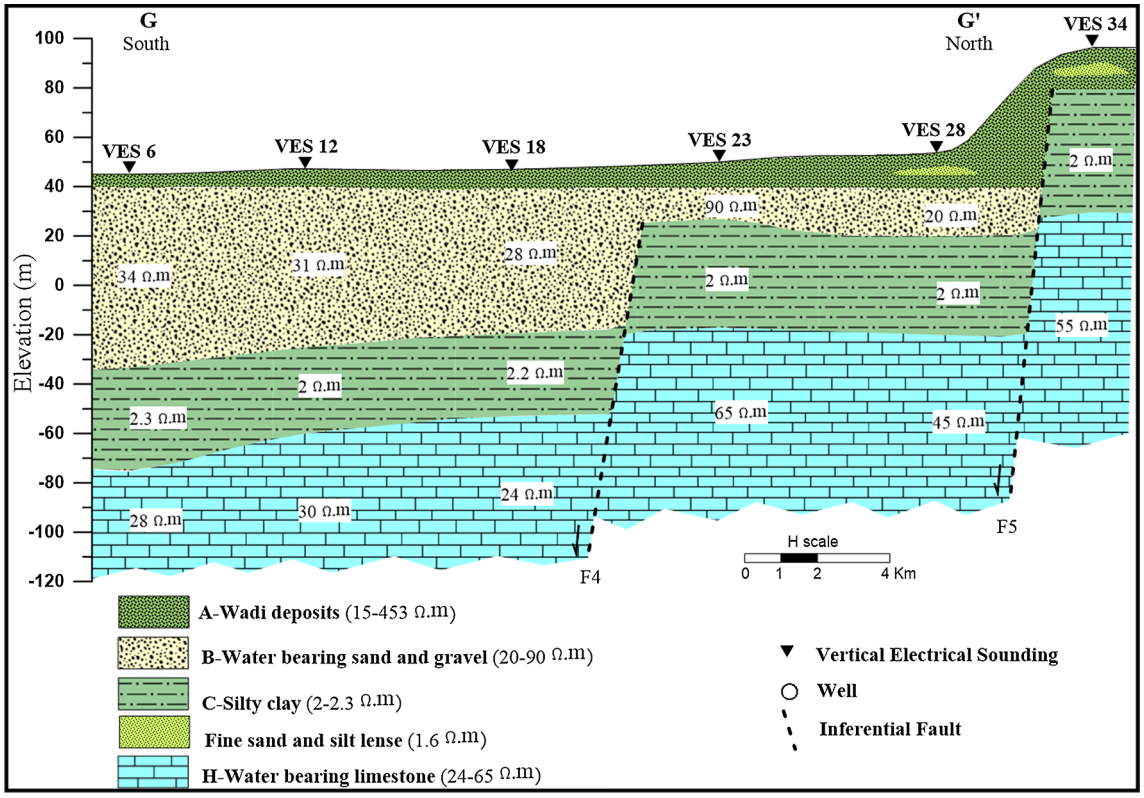

Fig. 23. Geoelectric resistivity cross-section G-G′.

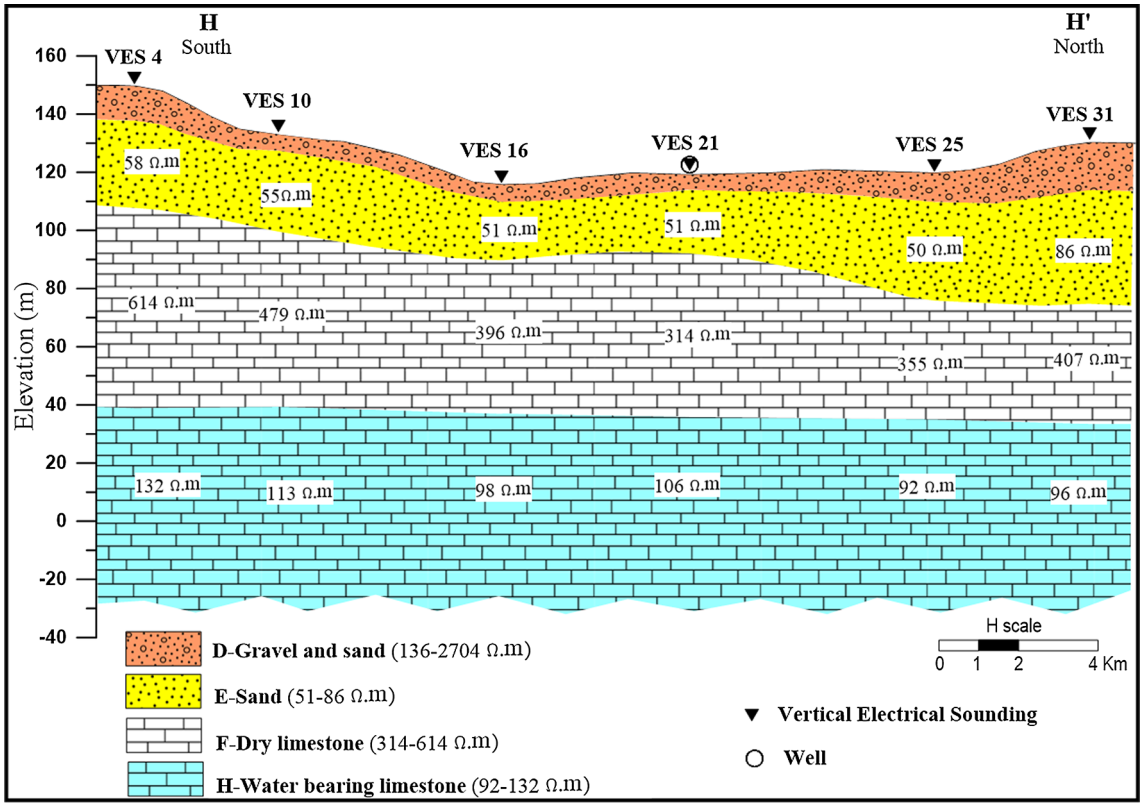

Fig. 24. Geoelectric resistivity cross-section H-H′.

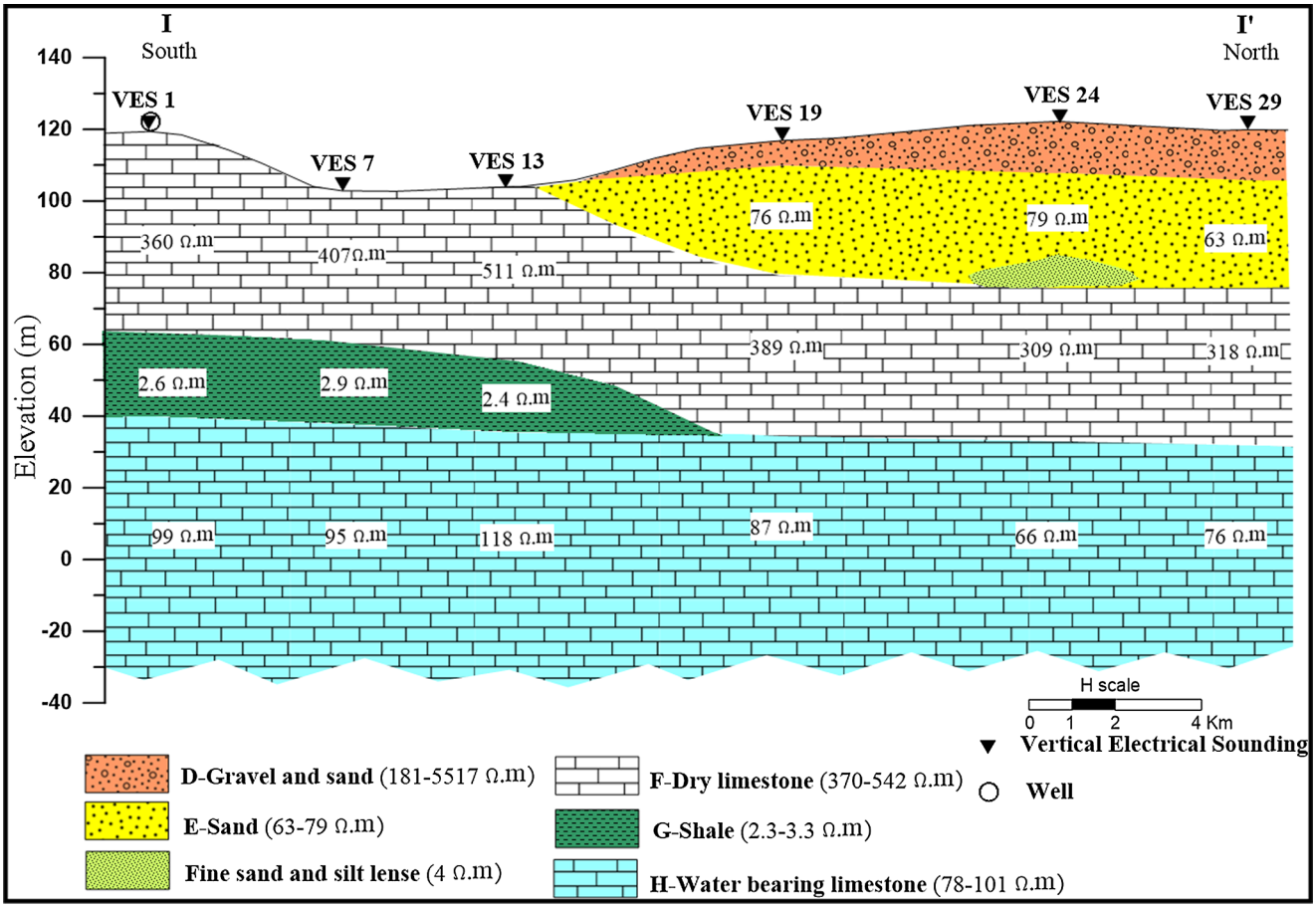

Fig. 25. Geoelectric resistivity cross-section I-I′.

Table 2
Resistivities, thicknesses ranges, and their related lithology.

Layer	Resistivity range (Ω m)	Thickness (m)	Age	Lithology
A	15–453	5 m at VES (6) – 13 m at VES (28)	Quaternary	Wadi deposits
B	20–90	13 m at VES (23) – 73 m at VES (6)		Water-bearing sand and gravel
C	2–2.3	34 m at VES (18) – 44 m at VES (23)		Silty clay
D	76–8228	5 m at VES (22) – 28 m at VES (33)		Gravel and sand
E	20–123	12 m at VES (22) – 90 m at VES (15)		Sand
F	309–614	40 m at VES (24) – 70 m at VES (2)	Eocene	Dry limestone
G	2.3–3.3	24 m at VES (13) – 27 m at VES (22)		Shale
H	24–132	–		Water-bearing limestone

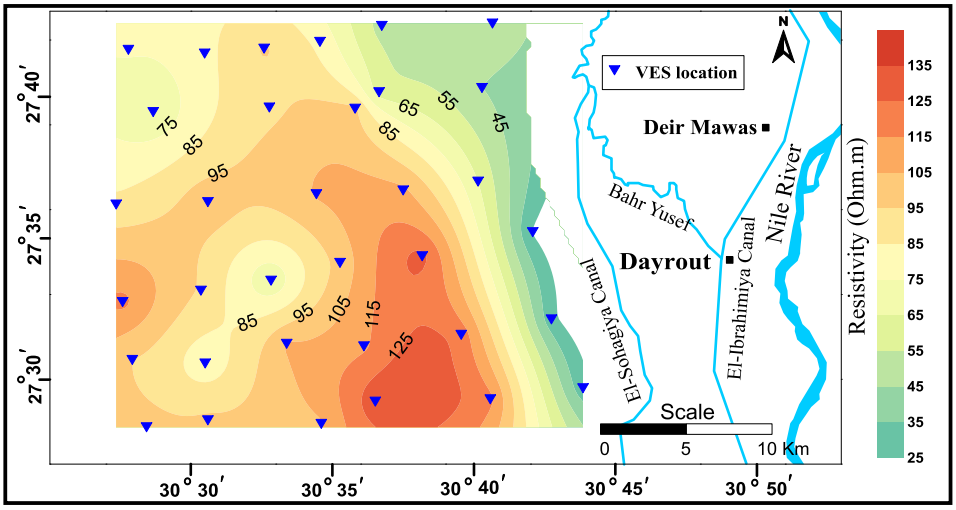

Fig. 26. True resistivity contour map of Eocene aquifer (Layer H).

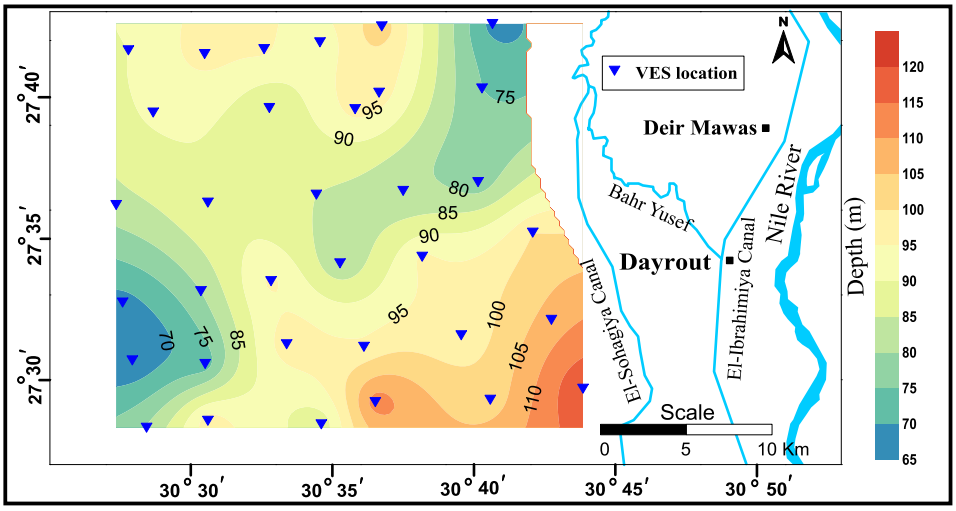

Fig. 27. Depth to Eocene aquifer (Layer H) contour map.

References

Abdel Fattah, Th, 1990. Depth of investigation and current penetration in Schlumberger configuration (field applications). Delta J. Sci., Tanta Univ. 14 (3), 1042–1054.

Abdel Moneim, A.A., Fernández-Álvarez, José Paulino, Abu El Ella, E.M., Masoud, A.M., 2016. Groundwater management at West El-Minia Desert Area, Egypt using numerical modeling. J. Geosci. Environ. Protect. 4, 66–76.

Abou Heleika, M.M., Niesner, E., 2008. Configuration of the limestone aquifers in the central part of Egypt using electrical measurements. Hydrogeol. J. 17, 433–446.

Alotaibi, A.M., AlAmri, A.M., 2007. Ground water potentialities of Wadi Malakan-Southern Makkah AlMokadash City, Saudi Arabia. Geophys. Soc. J. 5 (1), 101–116.

Conoco, 1987. Geological Map of Egypt 1: 500,000 NG 36 NW Asyut.

EZZ El-Deen, H.M., Abdel Rahman, A.A., Barseim, M.S., 2005. Geoelectrical study on the groundwater occurrence in the Area Southwest of Sidi Barrani, Northwestern Coast, Egypt. Geophys. Soc. J. 3 (1), 109–118.

Ibrahim, E.H., Shereef, M.R., El Galladi, A.A., Pederson, L.B., 2004. Geoelectric study on Quaternary groundwater aquifers in Northwest Sinai, Egypt. Geophys. Soc. J. 2 (1), 69–74.

IPI2win program, 2003. Resistivity Sounding Interpretation program, Moscow State University. Moscow, Russia Version 3.0.1.a 7.01.03 (1990–2003).

Mahmoud, H.H., Kotb, A.D., 2017. Impact of the geological structures on the groundwater potential using geophysical techniques in West Bani Mazar Area, El Minia-Western Desert, Egypt. J. Afr. Earth Sci. 130, 161–173.

Mohamaden, M.I., Abuo, Shagar S., Abdallah, G., 2009. Geoelectrical survey for groundwater exploration at the Asyuit Governorate, Nile Valley, Egypt. JKAU: Mar. Sci. 20, 91–108.

Mousa, S.A., 2003. The role of 1-D sounding and 2-D resistivity inversions in delineating the near-surface lithologic variations in Tushka area, south of Egypt. Geophys. Soc. J. 1, 57–64.

Salem, A.A., 2015. Hydrogeological studies on the shallow aquifers in the Area West Samalot El-Minia Governorate, Egypt. Egypt. J. Pure Appl. Sci. 53 (4), 49–60.

Said, R., 1990. The geology of Egypt. Consultant, annals, Virginia, USA and Cairo Egypt. p. 487–523.

Shabana, A.R., 2010. Hydrogeological Studies on the Area West Deir Mouas-Mallawi, El Minia Governorate, Egypt. Egypt. J. Geol. 54, 61–78.

Youssef, A.M.A., Abdellatief, T.A., Mousa, S.E., Tamamy, A.M., 2004. Geoelectrical Survey to Delineate the Extension of the Water Bearing Formations in Wadi Gharandal, Southwest Sinai, Egypt. Geophys. Soc. J. 2 (1), 75–84.

Youssef, M.I., 1968. Structural pattern of Egypt and its interpretation. Bull. Amer. Assoc. Petrol. Geol. 52 (4), 601–614.